Supplementary Information for

Guiding 3D cell migration in deformed synthetic hydrogel microstructures

Miriam Dietrich[1,2], Hugo Le Roy[3], David B. Brückner[4], Hanna Engelke[5], Roman Zantl[2], Joachim O. Rädler[1], Chase P. Broedersz[4]

[1] Faculty of Physics and Center for NanoScience, Ludwig-Maximilians-University, Munich, Germany
[2] ibidi GmbH, Martinsried, Germany
[3] École Normale supérieure Paris-Saclay, France
[4] Arnold-Sommerfeld Center for Theoretical Physics and Center for NanoScience, Ludwig-Maximilians-University, Munich, Germany
[5] Department of Chemistry and Center for NanoScience, Ludwig-Maximilians-University, Munich, Germany

1. Experimental system

Bulk stiffness measurements of hydrogel slabs

Bulk stiffness measurements of hydrogel slabs were performed on a MCR100 plate-plate rheometer (Anton Paar) in oscillating mode with a frequency of 10 rad/s. An amplitude sweep was performed and the storage modulus for every gel was calculated in the linear regime. The tested gels are soft, with gels containing 3 mM PEG-NB being more rigid than gels with the same cross-linker ratio containing only 2 mM PEG-NB (Figure S1). Similar low stiffnesses were previously measured for synthetic gels and biopolymer networks used for cell migration studies.[S1,S2]
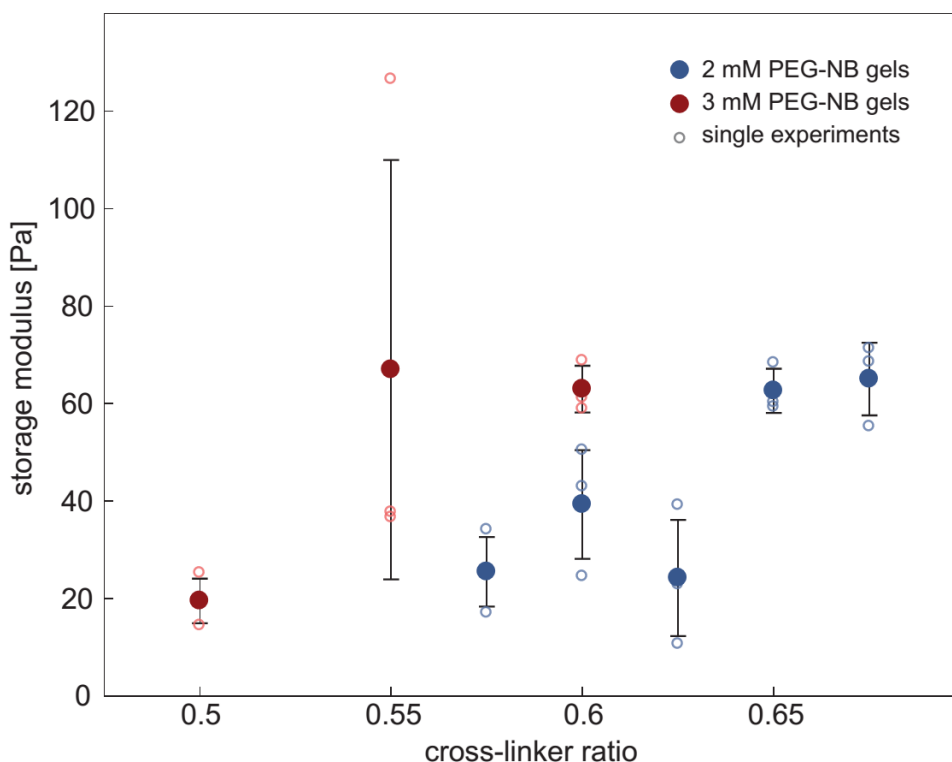
Figure S1: Bulk storage modulus of hydrogel slabs of different PEG-NB concentration and varying cross-linker ratio. Error bars represent the standard deviation obtained from 3 measurements.

Cell migration in isotropically swollen hydrogel slabs is isotropic

Migration of HT-1080 cells embedded in isotropically swollen hydrogels are monitored as described in the main text. To verify that cell migration in such hydrogels is isotropic, we calculate the anisotropic migration index (AMI) as described in the Materials and Methods part of the main text. In Figure S2, all tested hydrogels show an AMI close to zero, which indicates an isotropic migration behaviour of the cells.
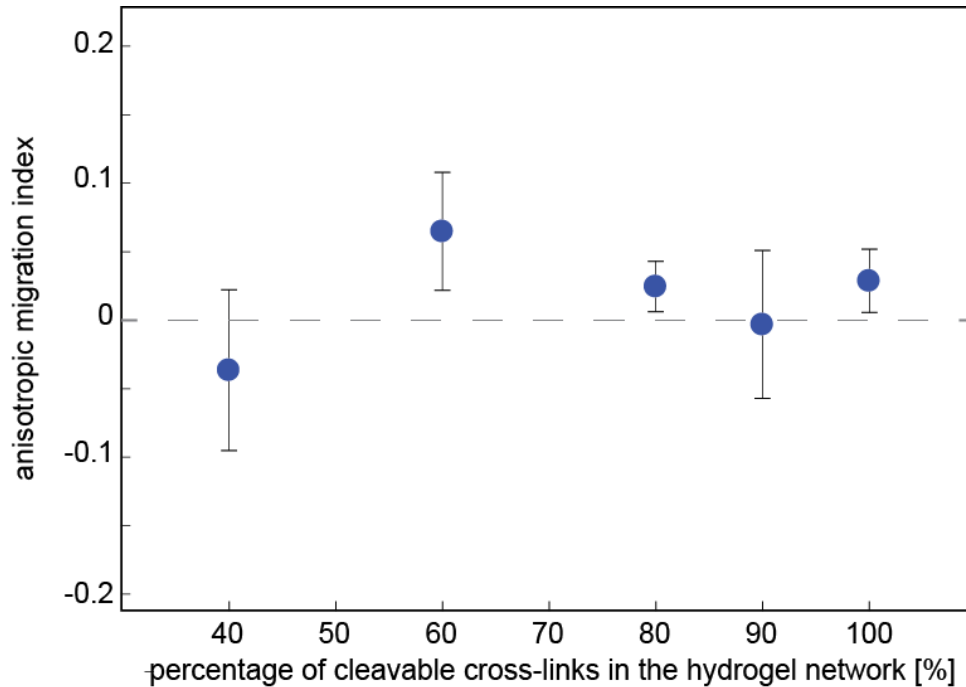
Figure S2: Quantification of the isotropic behaviour of HT-1080 cells migrating in isotropically swollen hydrogels of different degradability. Calculation of the anisotropic migration index is performed as described in the Material and Methods section of the main text. Error bars represent the standard deviation obtained from 3 measurements.

Analysis of the swelling behaviour of hydrogel microstructures in confinement

Polymerization of small hydrogel strips of high aspect ratio inside channel slides is achieved through photo-lithography. We use fluorescent time-lapse imaging together with Particle Image Velocimetry (PIV) (as described in the main text) to verify the uniaxial swelling of strips composed of different monomer and cross-linker concentrations (Figure S3). All compositions that we tested exhibit a uniaxial bead movement parallel to the strip width. For gels with low cross-linker concentration, an initial buckling of the structures (see Figure S4) results in slightly inhomogeneous velocity fields, because the swelling process starts immediately after polymerization, and fluorescent image acquisition can only be started when the unpolymerized hydrogel solution is flushed out of the system. Therefore, we cannot capture the very first swelling response of the strips. This is visible in the difference between Figure S4 A and B, where A shows the phase-contrast image after polymerization and B the first fluorescent image after washing the channel. However, in the course of the swelling, a straightened gel strip is achieved (see Figure S4 C + D).
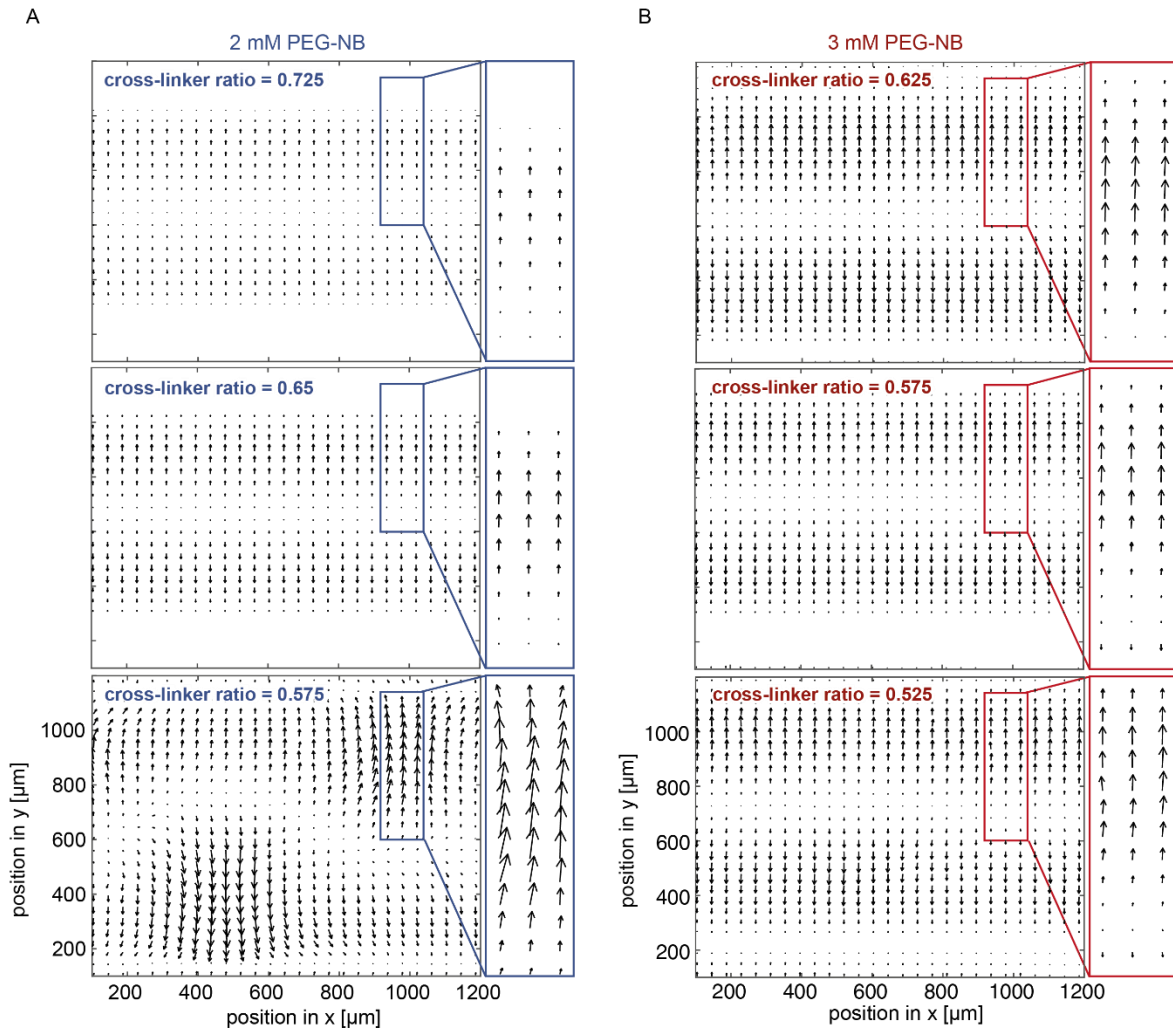
Figure S3: Velocity fields derived from PIV analysis using fluorescent microbeads. Gels containing 2 mM (A) and 3 mM (B) PEG-NB are tested with different cross-linker to monomer ratios as indicated in the different graphs.
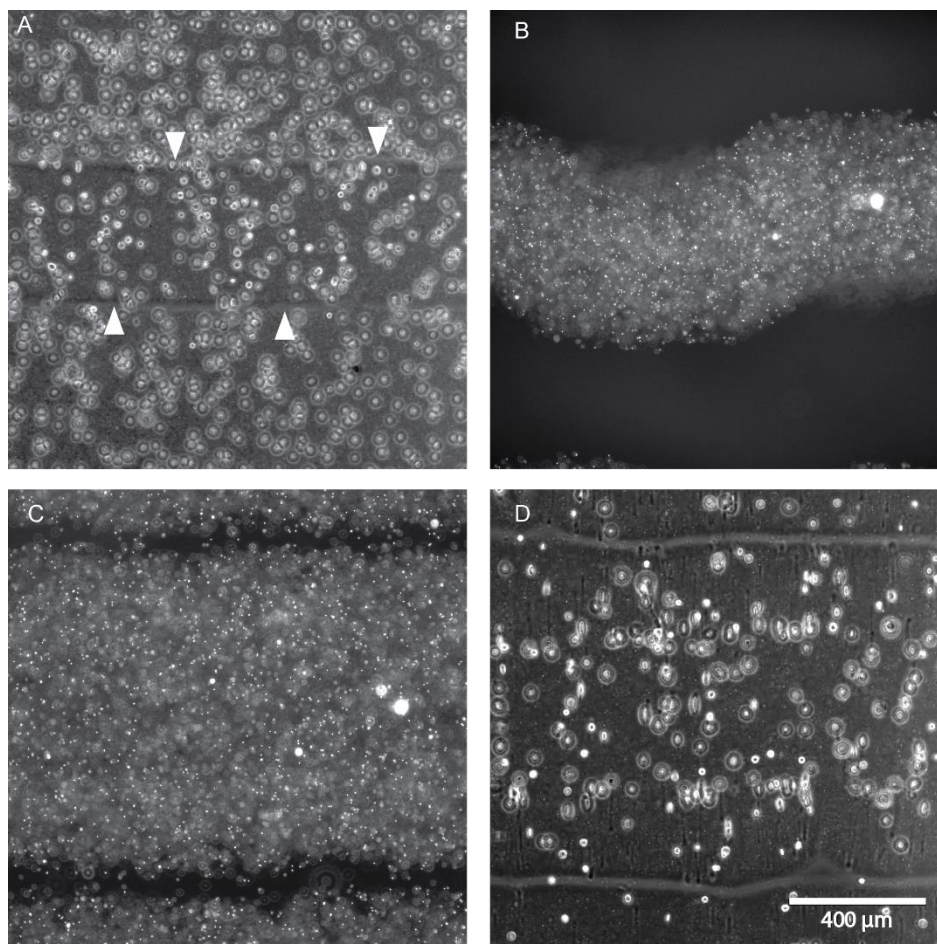
Figure S4: Swelling process in 2 mM hydrogel strips with a cross-linker ratio of 0.6. (A) Phase-contrast image of a 400 µm strip before swelling. Polymerized strip in the middle with borders marked by arrowheads. Unpolymerized solution is not washed out yet (upper and lower part of the image). (B) First fluorescent image used for PIV analysis of a strip with embedded fluorescent beads after washing (approximately 2 min after washing). The strip shows small initial bending. (C) Last fluorescent image of the PIV analysis after 2 h of swelling. (D) Phase-contrast image after swelling.

HT-1080 cell migration in uniaxially swollen hydrogel strips of different density

With our synthetic hydrogel system, we are able to vary the composition of the gel. Increasing the cross-linker ratio yields a more cross-linked gel with smaller mesh sizes. Therefore, migration in higher cross-linked gels is more challenging for cells and the percentage of migrating cells decreases. By also increasing the PEG-NB monomer concentration, the gel becomes even denser, which is the reason for the reduced number of migrating cells in 3 mM gels compared to 2 mM hydrogels of the same cross-linker ratio (see Figure S5).
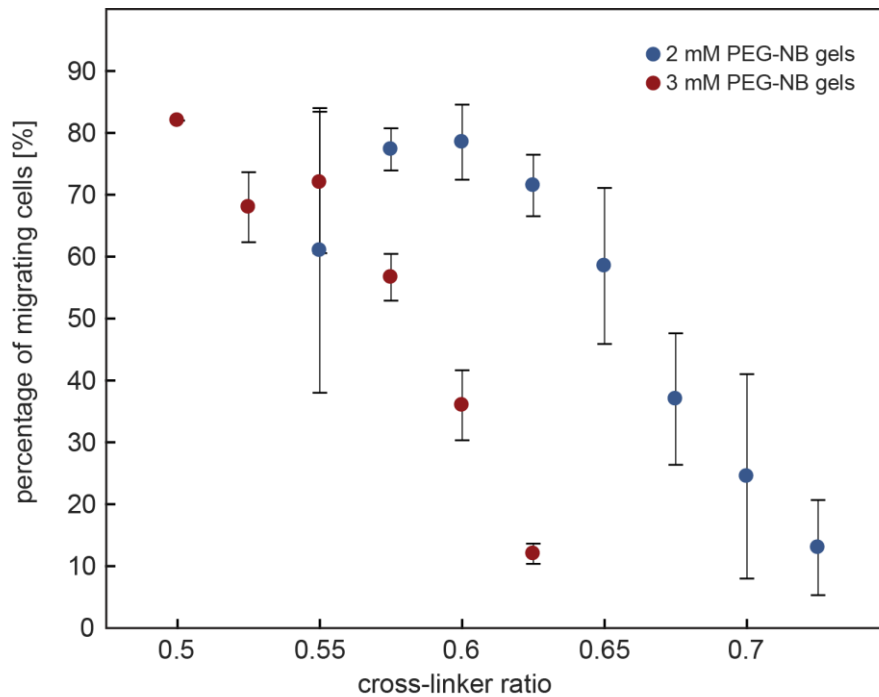
Figure S5: Percentage of HT-1080 cells migrating in 2 mM and 3 mM gels of different cross-linker ratio. Migrating cells are defined by a Euclidean distance of more than 40 µm migrated by the cell in 24 h. Error bars represent the standard deviation obtained from 3 measurements.

The migration of embedded HT-1080 cells in strained networks depends non-monotonically on the strain magnitude with the highest anisotropic migration at intermediate strain levels (see Figure 5 A of the main text). To elucidate if this anisotropic migration is accompanied by an alignment of cells to the external strain, we present a set of randomly selected cells under different strain conditions in Figure S6. Comparable to the migration directionality, cells at high strain magnitudes show less cell alignment parallel to the strain than cells at intermediate strains.
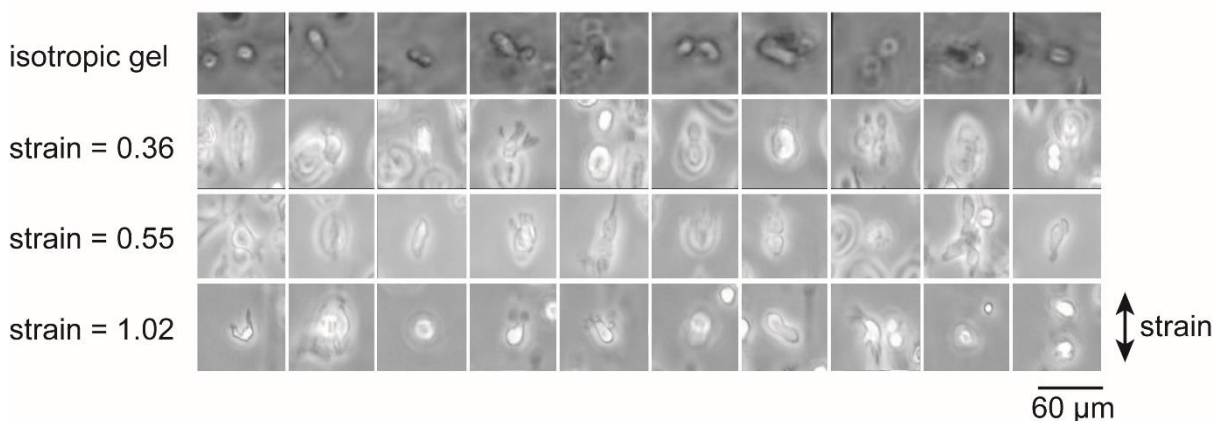
Figure S6: Example cells in gels of different swelling strain. 10 images of cells migrating in gels for 12 h were randomly selected to illustrate cell alignment to the strain direction. In the first row, cells in isotropically swollen gel slabs are shown as reference.

Description of our cell migration model

To model a durotactic cell that proteolytically migrates in a hydrogel, we developed a simple theoretical model. The network used in the simulation is a coarse-grained lattice network, which is composed of a triangular grid of nodes connected by simple linear springs. The elastic energy of the network is given by the Hamiltonian

$$H = \frac{k}{2} \sum_{i=0}^{N} \sum_{\langle ij \rangle} \left(\left| r_i - r_j \right| - l_0 \right)^2 , \tag{S1}$$

where r_i and r_j are the vector positions of the node i and its neighbours j, the sum runs over all nearest-neighbour pairs of nodes, and k is the elastic constant of the springs with the rest length l_0.

To introduce disorder in the otherwise regular network, we randomly remove spring connections with a certain probability *1-P*. Therefore, the average number of bonds Z connected to a node can be tuned as $Z = 6P$. Unless stated otherwise, an average connectivity of $Z = 4.8$ is used in all simulations. We chose this connectivity for all our simulations, because this choice results in a macroscopically rigid network. The cell in our simulation can move between lattice nodes to migrate through the network. The trajectory of the modelled cell is therefore a coarse-grained version of a real cell movement.

An important matrix property for a durotactic cell migrating in a network is the local matrix stiffness. In our model, the local network stiffness is associated with the network nodes. When a node i is displaced by a distance δx_ν in direction ν, the network responds with a restoring force $f_\mu^{(i)}(\delta x_\nu)$ in the direction μ. Therefore, we can associate a tensorial local stiffness $k_{\mu\nu}^{(i)}$ to every node i, defined as

$$k_{\mu\nu}^{(i)} = \frac{f_\mu^{(i)}(\delta x_\nu)}{\delta x_\nu} \tag{S2}$$

To simulate cell migration in the network, every migration step of a cell is composed of four basic steps in our model: In the first step, the cell pulls on the twelve second nearest nodes (yellow dots in Figure 3 B in the main text) and displaces them by a distance δx towards the cell centre. Next, the displacement of all network nodes due to the pulling is calculated by minimizing the elastic energy using a standard conjugate gradient algorithm. In addition, the restoring force F, which the network applies to each of the nodes, is computed to obtain the local stiffness according to Equation (S2). As a third step, the cell moves to the neighbouring node (grey nodes in Figure 3 B of the main text) with the highest stiffness magnitude $\bar{k}$, defined as

$$\bar{k} = \frac{\|F\|}{\|\delta l\|} \tag{S3}$$

In the last step, local proteolytic digestion of the matrix is simulated by a deletion of springs neighbouring the cell at a certain proteolytic rate r_p. For every simulated cell, 100 of these migration steps generate a cell migration trajectory, unless stated otherwise. To calibrate the simulated cell migration to the experimentally observed behaviour, we used isotropic networks to compare simulated and experimental migration statistics (see Figure 4 in the main text). With an average proteolysis rate of 1 deleted bond per computational cycle we achieve reasonable quantitative agreement. Therefore, this proteolysis rate was used for all further simulations of strained networks.

To simulate cell migration in externally strained matrices, we stretch the network prior to a cell migration simulation. Before stretching, the network is rotated by 15° to prevent an alignment of the stretch direction with special lattice directions. Because the lattice axis is not aligned with the external deformation direction, node stiffness probed at an angle of 7° and 97° are referred to as "parallel" and "perpendicular" to the deformation, respectively.

In Figure S7 we show the mean squared displacement (MSD) of cells migrating in strained networks and compare the behaviour of HT-1080 cells embedded in gels of two different PEG-NB concentrations with simulated cell migration. For the experiments, cell migration data of gels with different strains were binned to increase cell number for each sample. The MSD increases with time as an approximate power law with an exponent of around 1.4 for the experiments and simulation for all strains tested. This is in good agreement with our migration analysis in isotropic gels. For experimental data, cells migrating in higher cross-linked and therefore less strained networks show an overall decreased MSD indicating less migration in these networks.
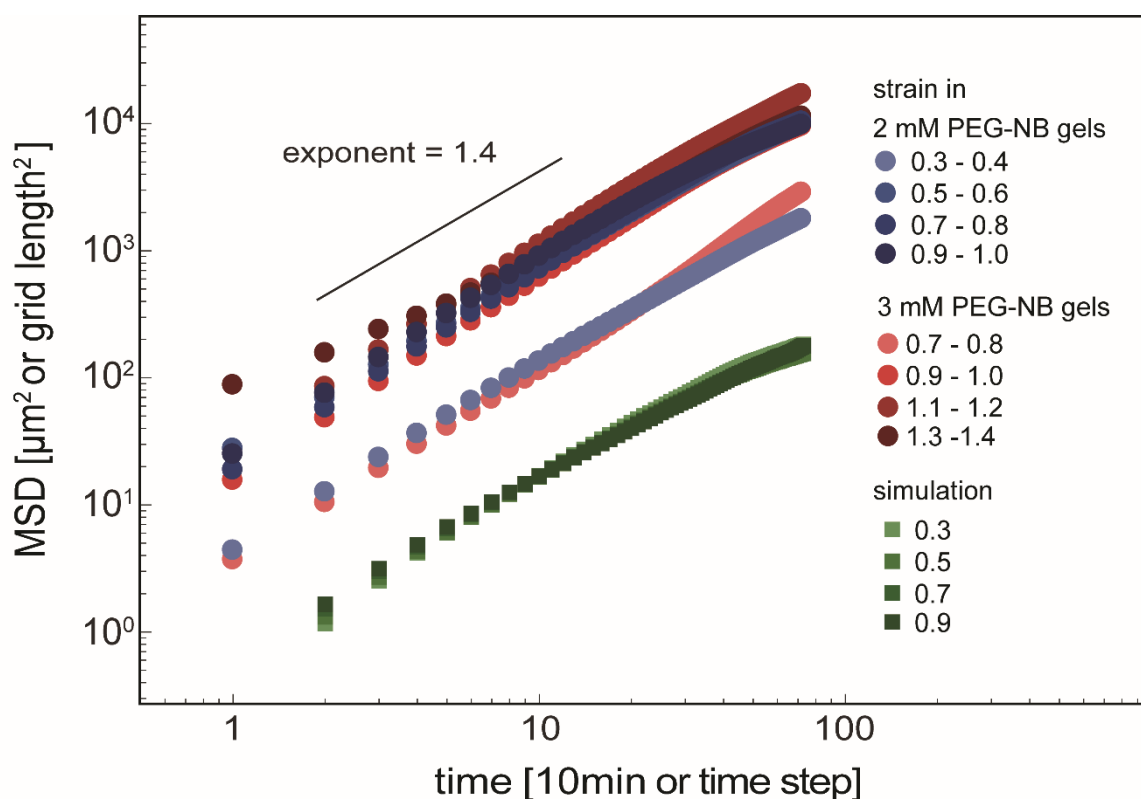
Figure S7: Analysis of cell migration in networks of varying strain. Mean squared displacement (MSD) of experiments binned for strain increments of 0.1 displayed as circles (2 mM PEG-NB gels in blue, 3 mM PEG-NB gels in red), simulated data displayed as green squares.

Figure 5 C of the main text shows the initial matrix node stiffness $\bar{k}$ of the simulated network, calculated according to Equation (S3) and normalized to the stiffness at zero strain, for different external strain levels. Figure S8 shows the normalized node stiffness measured while a cell migrates in the network and digests cross-links. This digestion changes the stiffness of the matrix nodes only to a small extent.
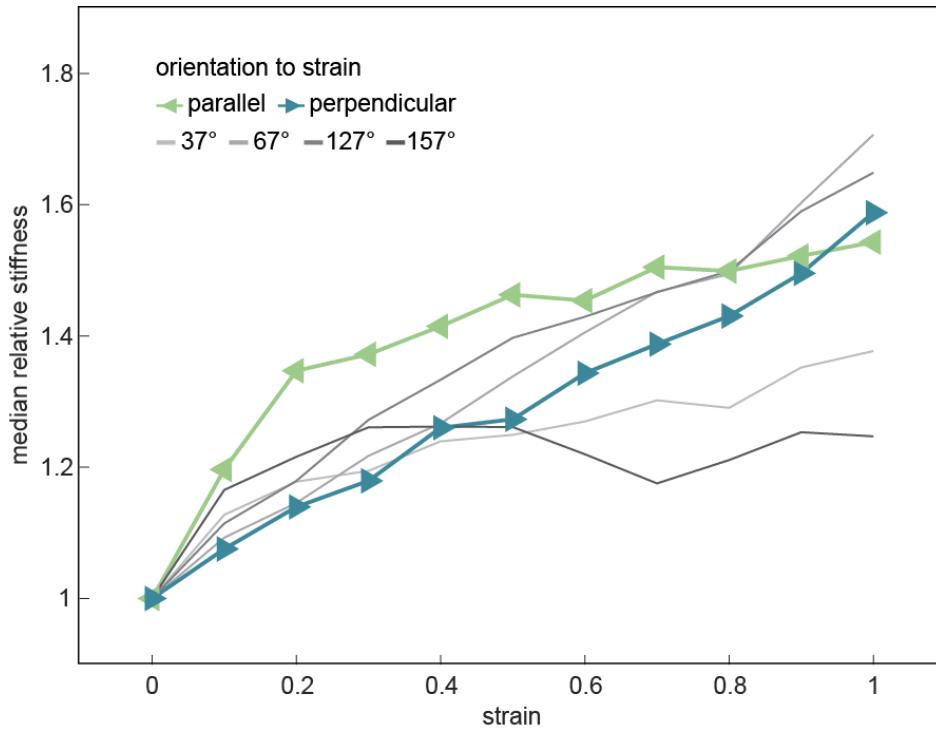
Figure S8: Median node stiffness measured by cells migrating in a strained network. The node stiffness measured by the cell in different orientations to the strain direction is recorded and normalized to the stiffness at zero strain.

Addition of time-averaged mechanosensing in the durotactic cell migration simulation

We investigated if the addition of an effective cell polarization component in the simulation increases the achieved maximal anisotropic cell migration parallel to the external strain direction. First, we note that cell polarization or persistence will not affect the magnitude of migration anisotropy, unless the polarization itself is strain or stiffness sensitive. Therefore, we alter the durotactic decision process of the cell. Instead of measuring the local stiffness in one computational cycle and migrating in the direction of highest stiffness, we assume that the cell responds to the average of the N_{av} most recent stiffness measurements to determine the migration direction of the cell. Note, this time-averaged mechanosensing will lead to more persistent motion. A total of 50 migration steps are simulated for every cell with 200 simulated cells per condition. For the calculation of the AMI according to Equation (2) of the main text, only migration steps after an initial N_{av} steps are used.

In Figure S9, the AMI of cells migrating in 30% strained networks increases with increasing N_{av}. For $N_{av} = 30$ we observe values similar to the experimental maximal AMI.
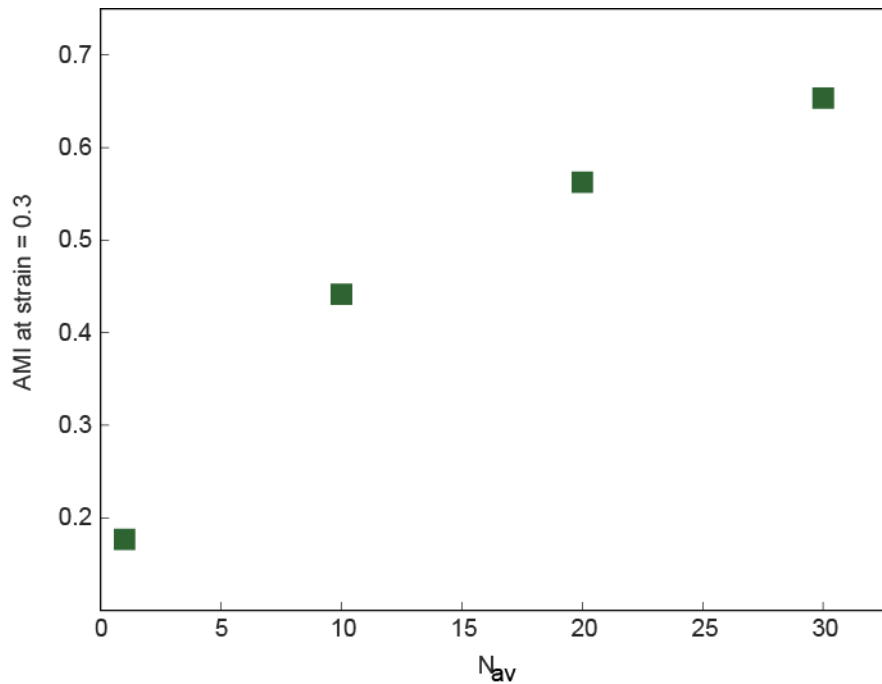
Figure S9: AMI at a strain of 0.3 for cell migration simulations with time-averaged mechanosensing. Durotactic migration in the polarized migration model is based on the average of the last N_{av} stiffness measurements.

Supplemental movies

Supplemental movie S1: HT-1080 cells migrating in a 100% degradable hydrogel.

HT-1080 cells embedded in a hydrogel with a PEG-NB monomer concentration of 2 mM and a cross-linker ratio of 0.6. Every cross-link consists of a peptide sequence which can be proteolytically cleaved by matrix-metalloproteinases to enable cell migration in the gel.

Supplemental movie S2: HT-1080 cells migrating in an 80% degradable hydrogel.

HT-1080 cells embedded in a hydrogel with a PEG-NB monomer concentration of 2 mM and a cross-linker ratio of 0.6. 80% of the cross-links consists of a peptide sequence which can be proteolytically cleaved by matrix-metalloproteinases to enable cell migration in the gel. 20% of the cross-links are proteolytically stable PEG-cross-links which reduces the overall ability of cells to migrate through the network.

Supplemental movie S3: HT-1080 cells migrating in a 40% degradable hydrogel.

HT-1080 cells embedded in a hydrogel with a PEG-NB monomer concentration of 2 mM and a cross-linker ratio of 0.6. Only 40% of the cross-links consists of a peptide sequence which can be proteolytically cleaved by matrix-metalloproteinases to enable cell migration in the gel. 60% of the cross-links are proteolytically stable PEG-cross-links which reduces the overall ability of cells to migrate through the network.

Supplemental movie S4: Anisotropic swelling of a hydrogel strip in a confinement

Fluorescent beads are embedded in the hydrogel to visualize the swelling process of a hydrogel strip, consisting of 2 mM PEG-NB and a cross-linker ratio of 0.65. Such image sequences are used for Particle Image Velocimetry (PIV) to analyse the swelling process and verify the induction of uniaxial strain in the hydrogel.

Supplemental movie S5: HT-1080 cells migrating in a strained hydrogel strip with strain = 0.45

HT-1080 cells embedded in a hydrogel strip with a PEG-NB monomer concentration of 2 mM and a cross-linker ratio of 0.65. A strain of 0.45 is induced in the hydrogel structure.

Supplemental movie S6: HT-1080 cells migrating in a strained hydrogel strip with strain = 0.72

HT-1080 cells embedded in a hydrogel strip with a PEG-NB monomer concentration of 2 mM and a cross-linker ratio of 0.65. A strain of 0.72 is induced in the hydrogel structure.

Supplemental movie S7: Simulation of a cell moving on an unstrained strained network

Example simulation of a cell moving in an isotropic lattice network of linear springs for 100 simulated migration steps.

Supplemental movie S8: Simulation of a cell moving on a strained network with strain = 0.3

Example simulation of a cell moving in a strained lattice network (strain = 0.3) of linear springs for 100 simulated migration steps.

Supplemental movie S9: Simulation of a cell moving on a strained network with strain = 0.9

Example simulation of a cell moving in a strained lattice network (strain = 0.9) of linear springs for 100 simulated migration steps.

References for the supplementary information

S1 S. P. Singh, M. P. Schwartz, J. Y. Lee, B. D. Fairbanks and K. S. Anseth, Biomater. Sci., 2014, 2, 1024–1034.

S2 G. P. Raeber, M. P. Lutolf and J. A. Hubbell, Acta Biomater., 2007, 3, 615–629.